Title: Novel HDAC6 inhibitors increase tubulin acetylation and rescue axonal transport of mitochondria in a model of Charcot-Marie-Tooth Type 2F.

Authors: Robert Adalbert†¶||, Akira Kaieda‡, Christina Antoniou†, Andrea Loreto†, Xiuna Yang†, Jonathan Gilley†, Takashi Hoshino‡, Keiko Uga‡[#], Mahindra T. Makhija‡ and Michael P. Coleman†[§]

Affiliation:

†John van Geest Centre for Brain Repair, Department of Clinical Neurosciences, University of Cambridge, Forvie Site, Robinson Way, Cambridge CB2 0PY, UK

‡Takeda Pharmaceutical Company Limited, 26-1, Muraoka-higashi 2-chome, Fujisawa, Kanagawa 251-8555, Japan

‡Takeda Development Centre Europe Ltd., 61 Aldwych London WC2B 4AE UK

[§]Babraham Institute, Babraham, Cambridge, CB22 3AT, UK

[||]Department of Anatomy, Histology and Embryology, Faculty of Medicine, University of Szeged, Szeged, Hungary

¶ Present address: Comparative Neuromuscular Disease Laboratory, Royal Veterinary College, 4 Royal College Street, Camden, London NW1 0TU, UK

[#]**Present address:** Axcelead Drug Discovery Partners, Inc., 26-1, Muraoka-higashi 2-chome, Fujisawa, Kanagawa 251-0012, Japan

ABSTRACT

Disruption of axonal transport causes a number of rare, inherited axonopathies and is heavily implicated in a wide range of more common neurodegenerative disorders, many of them age-related. Acetylation of α-tubulin is one important regulatory mechanism, influencing microtubule stability and motor protein attachment. Of several strategies so far used to enhance axonal transport, increasing microtubule acetylation through inhibition of the deacetylase enzyme HDAC6 has been one of the most effective. Several inhibitors have been developed and tested in animal and cellular models but better drug candidates are still needed. Here we report the development and characterisation of two highly potent HDAC6 inhibitors, which show low toxicity, promising pharmacokinetic properties, and enhance microtubule acetylation in the nanomolar range. We demonstrate their capacity to rescue axonal transport of mitochondria in a primary neuronal culture model of the inherited axonopathy Charcot-Marie-Tooth Type 2F, caused by a dominantly acting mutation in heat shock protein beta 1.

Keywords: HDAC6; CMT; Axonal transport; Mitochondria, Axonopathy, α-tubulin.

INTRODUCTION

The bidirectional movement of macromolecules and organelles along axons is essential for axon survival and function, and requires a complex machinery involving motor proteins, adapters coupling to specific cargoes, microtubule tracks and regulators of all the above. Not surprisingly, such an essential process involving many components can malfunction in a number of ways and when it does the consequences can be profound. Mutation of genes encoding axonal transport machinery and regulators cause a number of axonopathies, and especially diseases of long axons. For example, mutations in KIF5A encoding a major anterograde motor protein are an established cause of hereditary spastic paraplegia SPG10

[1], and have also been linked to Charcot-Marie-Tooth Disease type 2 (CMT2) [2], amyotrophic lateral sclerosis (ALS) [3, 4] and neonatal intractable myoclonus [5]. Mutant dynactin causes motor neuron disease and distal spinal and bulbar muscular atrophy [6, 7] and in mice the mutation of tubulin chaperone protein Tbce causes a severe, early onset loss of motor axons with a major deficiency of microtubules [8].

Charcot-Marie-Tooth Disease type 2 (CMT2) is an axonal, non-demyelinating peripheral neuropathy characterized by distal muscle weakness and atrophy, mild sensory loss, and normal or near-normal nerve conduction velocities [9]. The Charcot-Marie-Tooth disease subtype 2F (CMT2F) and distal hereditary motor neuropathy subtype 2B (dHMN2B) are caused by autosomal dominantly inherited mutations in the small heat shock protein B1 (*HSPB1*) gene [10, 11]. The gene codes for heat shock protein beta-1 (HSPB1, also known as HSP27), which is a member of the small heat shock protein family comprising a highly conserved α-crystalline domain. HSPB1 acts as a chaperone binding with partially denatured proteins to prevent aggregation [12, 13]. Up to now, 18 mutations in *HSPB1* have been linked to CMT2F and 27 mutations to dHMN 2 [14]. The S135F and P182L mutations are among the best characterized mutations so far [11, 15, 16]. The S135F mutation is the only one that causes both CMT2 and dHMN2B. P182L mutation is associated only with dHMN2B [15]. The S135F mutation is located in the α-crystallin domain while P182L mutation lies in the short C-terminal tail of the protein [15]. Interestingly the localization of the mutation was shown to have different effects on the protein function. While the S135F mutation caused the protein to increase its chaperone activity accompanied with an increased in its monomeric state the chaperone activity of HSPB1 was not affected by the P182L mutation [17].

Four mutant *HSPB1* transgenic mouse models of CMT2F and/or dHMN2B have been developed so far, which partially recapitulate the hallmarks of peripheral neuropathy [11, 18-20].

S135F and P182L transgenic mice generated by d'Ydewalle et al. demonstrated noticeable phenotypes, the latter presents more like dHMN2B than CMT2F with a lack of sensory

symptoms [11] which recapitulates all key features of CMT2F or distal HMN2B, dependent on the mutation. However, CMT2F mouse models generated by other groups had notable differences. S135F transgenic mice reported by Lee et al. had no sensory phenotype and presented only a strict motor loss, similar to the P182L, but not the S135F mice of d'Ydewalle et al [18]. In further contrast, the R136W mouse model did not demonstrate any functional or behavioral deficits [20]. When R127W and P182L mutant proteins were expressed at physiological levels to alleviate concerns of artifacts due to overexpression, no pathology and behavioural deficits were found in mice [19]. This could be due to insufficient expression of HSPB1 under the ROSA26 locus.

In addition to rare disorders and animal models, axonal transport deficiency is heavily implicated in many more common neurodegenerative and axonal disorders. Several cancer chemotherapeutics that cause peripheral neuropathy as a dose-limiting complication target microtubules [21] and disrupt axonal transport [22]. In Alzheimer's disease, aggregation of microtubule associated protein tau, whose normal functions include regulation of microtubule stability and motor protein attachment [23, 24] plays a prominent role, exogenously applied $A\beta_{1-42}$ is able to disrupt axonal transport in a tau-dependent manner [25]. The two may also interact [26] and impairment of axonal transport exacerbates animal models [27]. There are many indications of a wider role also in ALS [28], Huntington's disease [29], Parkinsonism and frontotemporal dementia [30, 31], and normal ageing, the biggest risk factor in each of these [32], is accompanied by a twofold decline in axonal transport [33]. Thus, rare but often better-understood inherited disorders involving an axonal transport mechanism are an important starting point to develop therapies that could have far wider application in neurodegenerative disease.

Axonal microtubules exist in a state of dynamic instability [34, 35], constantly both growing and severing to maintain them typically between 0.15-20 μm in length [36]. Acetylation of α-tubulin at Lys40 is reported to increase microtubule stability under mechanical stress [37] and to influence severing by katanin [38]. It also enhances the binding of kinesin-1 and axonal transport

[39, 40]. Beside SIRT2 [41] HDAC6 is the other major deacetylase for α-tubulin and its inhibition increases axonal transport of some cargoes in models of Charcot-Marie-Tooth disease types 2F [11] and 2D [42], ALS [43], and Vincristine neuropathy [44], also alleviating some symptoms. Beneficial outcomes have also been reported in models of Alzheimer's disease [45] and stroke [46] . Early studies of HDAC6 inhibition used tubacin, whose high lipophilicity and short *in vivo* half-life limited its usefulness. This was largely superseded by the development of Tubastatin A [47]. However, further improvement of potency is possible [48, 49] so it is important to develop new compounds targeting HDAC6 with greater potential for clinical application.

The HDAC inhibitors share a well-recognized pharmacophore that consists of three parts: a zinc binding group (ZBG), a linker, and a cap moiety. Classical HDAC inhibitors typically have the hydroxamic acid moiety as ZBG but the hydroxamic acid causes poor pharmacokinetics, low selectivity profiles, and production of active metabolites [50]. These features of hydroxamic acid are red flags for drug discovery in chronic diseases that are not life threatening**.** Therefore, we focussed here on the discovery of non-hydroxamic acid derivatives. High throughput screening (HTS) with a Takeda internal library provided several non-hydroxamic acid derivatives as hit compounds against HDAC6. By our medicinal chemistry efforts, we developed two compounds T-3796106 and T-3793168 that are highly selective for HDAC6, show CNS penetration and low toxicity both *in vivo* and *in vitro*. We report their dose-response effects for α-tubulin acetylation in primary neuronal cultures and their influence on axonal transport of mitochondria in a primary culture model of CMT2F.

RESULTS

Evaluation of inhibitory potencies (IC_{50}) of T-3796106 and T-3793168

The inhibitory potencies (IC_{50}) of T-3796106 and T-3793168, which were developed through medicinal chemistry campaign from HTS hit compounds, were evaluated in HDAC panel assay (Table 1). T-3796106 showed potent inhibitory activity against HDAC6 with the IC_{50} value of

12 nM. IC_{50} values for HDAC3, HDAC8, HDAC5, HDAC7, and HDAC9 were in the range of 1,000-3,000 nM. IC_{50} values for HDAC1 and HDAC4 were over 6,000 nM. T-3796106 did not show inhibitory activity against HDAC2, HDAC10, and HDAC11 up to 10,000 nM. IC_{50} values of T-3793168 were 86 nM for HDAC6 and over 2,000 nM against other HDACs.

Target	Compounds IC_{50} (nM)[a]		
	T-3796106	T-3793168	Tubastatin A
HDAC1	6200 (5820-6660)	[b]	>10000
HDAC2	>10000	[b]	>10000
HDAC3	4000 (3480-4470)	[b]	>10000
HDAC8	>1000	5600 (4170-7080)	>1000
HDAC4	6200 (5970-6380)	>10000	6200 (6030-6330)
HDAC5	1700 (1610-1800)	2300 (1550-3060)	1900 (1580-2310)
HDAC7	1100 (1050-1130)	5800 (4000-7660)	590 (530-641)
HDAC9	2700 (2540-2840)	5000 (4950-4960)	1100 (913-1380)
HDAC6	12 (12.3-12.4)	86 (67.4-104)	15 (14.3-15.2)
HDAC10	>10000	[b]	>10000
HDAC11	>10000	[b]	>10000

Table 1 HDAC panel assay. The selectivity of T-3796106 and T-3793168 was analyzed based on HDAC enzyme inhibition. [a] The compound activity against 11 HDACs represented with the IC_{50} value. The IC_{50} values shown are the mean values of duplicate measurements; the numbers in parentheses represent each data. [b] No inhibition or compound activity that could not be fit to an IC_{50} curve.

T-3796106 and T-3793168 do not cause neuronal toxicity even at high concentrations

First, we tested whether T-3796106 or T-3793168 induces any cytotoxicity in murine neuronal explant cultures, using concentrations substantially higher than those we subsequently used

for axonal transport studies to indicate a large therapeutic window. We used superior cervical ganglion (SCG) explants because this neuron type is well-suited for genetic manipulation by microinjection and for axonal transport studies [51, 52], and incubated with concentrations from 1 μM to 100 μM for 24 h. No toxicity was observed at any concentration. Neurites remained morphologically similar to vehicle-treated or untreated cultures, even in their distal terminals which are typically the most vulnerable site (Fig 1A, B). Thus, both compounds are safe for neurons up to 100 μM for at least 24 h.

Increased acetylation levels of α-tubulin after T-3796106 and T-3793168 treatment in neurons

We next confirmed that steady state α-tubulin acetylation increases with either T-3796106 or T-3793168 within the above concentration range (data not shown), before titrating down to determine the dose-response curve for α-tubulin acetylation at sub-saturating levels, thereby minimizing the risk of off-target effects. Both compounds showed a clear dose-response effect between 1 nM and 250 nM in a 24 h incubation (Fig 2A), reaching significance at 50 nM for T-3796106 and 250 nM for T-3793168 (Fig 2B). Based on this characterization we used concentrations of 100 nM and 250 nM respectively in our subsequent axonal transport experiments. At these concentrations, there was no effect on histone acetylation which indicates a high selectivity of these compounds towards HDAC6 (Supplementary Figure 1).

Axonal transport of mitochondria in wild type SCG cultures is not altered by T-3796106 or T-3793168

In the absence of a pathogenic mutation, we found no significant change in either the number or the average and maximum velocity of axonally transported mitochondria in dissociated wild-type SCG neurons treated with T-3796106, T-3793168 or Tubastatin A (Fig 3B, C, D, E). Thus, there is no change in basal axonal transport parameters for this cargo.

Mitochondrial transport impairment induced by S135F mutation is rescued by T-3793168

In the presence of the HSPB1^{S135F} mutation, which causes CMT2 and distal HMN in patients [15], both the numbers of anterogradely and retrogradely moving mitochondria were significantly decreased relative to wild type neurons 12 h after microinjection (Fig 4A, B), mirroring similar changes reported in sensory neurons [11]. The transport deficits in both directions were significantly rescued in neurons treated for 24 h with 250 nM T-3793168, while those treated with 100 nM compound T-3796106 showed a trend towards increased mitochondrial transport but the difference was not statistically significant (Fig 4A, B). As previously reported [11], we also found a rescue of anterograde axonal transport with 1 μM Tubastatin A, but in the retrograde direction the trend towards a rescue with Tubastatin A was not significant. The average and maximum speed of mitochondria movement was not significantly altered in the neurons with the HSPB1^{S135F} mutation and was unaffected by any of these treatments (Fig 4C, D).

P182L mutation does not alter mitochondrial transport in SCG neurons

Consistent with previous findings in sensory neurons [11], SCG neurons expressing HSPB1^{P182L} showed no significant changes in mitochondrial transport compared to wild type neurons (Fig 5). Treatment of these mutant-expressing neurons with T-3796106, T-3793168 or Tubastatin A also had no effect on mitochondrial movement (Fig 5).

T-3796106 and T-3793168 increase α-tubulin acetylation in human whole blood

We finally investigated the effects of T-3796106 and T-3793168 on acetylation of α-tubulin in human cells, using whole blood. For both compounds, clear dose-response effects were observed between 10 nM and 30 μM in a 4 h incubation (Fig 6). Over 100 μM of our compounds and 300 μM of hydroxamic acid-based HDAC6 inhibitor ACY-1215 showed some precipitate when the compounds were added in the culture medium. We also observed the effect of Tubastatin A on acetylated a-tubulin in the human whole blood assay. It showed a similar trend. In brief, the levels of acetylated a-tubulin were almost the same at 10 and 30 μM of Tubastatin A (data not shown) as well as that of ACY-1215.

DISCUSSION

We report the development and characterization of two novel non-hydroxamic acid-based inhibitors with high potency and specificity for HDAC6, low toxicity in murine primary neuronal cultures and a dose-dependent effect on neuronal α-tubulin acetylation between 1-250 nM. T-3793168 significantly increases both the anterograde and retrograde flux of mitochondria in axonal transport within 24 h of application to neurons expressing the CMT-2F HSPB1 mutation S135F, and T-3796106 shows a similar, albeit non-significant trend. Neither alters axonal transport in wild-type cells.

For both compounds the changes in acetylated tubulin in whole blood was several orders of magnitude greater than those in mouse primary neuronal cultures. This suggests a tissue-, tubulin isoform-, or species-specific effect on the efficacy of these HDAC6 inhibitors indicating significant scope of lead compound optimization. Further studies to understand the basis of this specificity should help to optimize their efficacies to achieve substantial enhancement of axonal transport in human axonal disorders.

A major advantage over hydroxamic acid-based inhibitors is greater selectivity over other HDAC family members and this is the case for these compounds. For example, hydroxamic acid-based HDAC6 inhibitor ACY-1215 has a high HDAC6 enzyme potency with IC_{50} value of 4.7 nM but much lower selectivity (12-fold selectivity for HDAC6 and HDAC1 at IC_{50}) [53]. In contrast, non-hydroxamic acid-based HDAC6 inhibitors T-3796106 and T-3793168 showed excellent selectivity (>25-fold over other HDAC family members; >100-fold selectivity over HDAC1 at IC_{50}).

It will be important now to test the effect of these compounds on axonal transport in other disease models where transport is impaired and the effect on other axonal transport cargoes. For example, axonal transport defects underlie vincristine neuropathy and some forms of hereditary spastic paraplegia and ALS, and have also been implicated in glaucoma,

Alzheimer's disease and multiple sclerosis. Many axonal transport cargoes need to be continuously shuttled back and forth but among some of the most important ones are NMNAT2, whose absence limits the survival of transected axons [51] and the retrograde transport of lysosomes to maintain efficient autophagy and mitochondrial quality control [54], and neurotrophins.

Finally, it will be important to test the efficacy of HDAC6 inhibition and rescue of axonal transport *in vivo* using methods for live imaging of transport cargoes in live nerves and CNS tissue [33, 55, 56], to assess how HDAC6 inhibition compares to other methods of boosting axonal transport in experimental models [57, 58] and to further develop these lead compounds.

METHODS

Chemicals

T-3796106 and T-3793168 are novel HDAC6 inhibitors developed by Takeda Pharmaceutical Company Limited (Patent WO2017014321)[59].The purity of T-3796106 and T-3793168 was determined to be ≥ 95% by elemental analysis which was performed by Sumika Chemical Analysis Service, Ltd. experimentally determined hydrogen, carbon, and nitrogen composition by elemental analysis was within ±0.4% of the expected value, implying a purity of ≥ 95%. ACY-1215 was synthesized and determined to be ≥ 95% purity by elemental analysis by Takeda Pharmaceutical Company Limited.

Enzyme assay

HDAC panel assay was performed by Reaction Biology Corp. (Malvern, PA, USA) according to their validated protocol. To evaluate the potency and selectivity of T-3796106 and T-3793168, HDAC panel assay was carried out by Reaction Biology Corp. Briefly, the deacetylation reaction was performed in buffer conditions of 50 mM Tris-HCl pH 8.0, 137 mM NaCl, 2.7 mM KCl, 1 mM $MgCl_2$, and 1 mg/mL bovine serum albumin (BSA), and 1%DMSO.

The fluorogenic peptide, RHK-K(Ac)-AMC, is used as substrate for Class1 and 2B HDACs, RHK(Ac)K(Ac)-AMC for HDAC8, and Boc-Lys(trifluoroacetyl)-AMC for Class2A HDACs. After the reaction, by Developer with Trichostatin A, a fluorescence signal (Ex. 360 nm/Em. 460 nm) developed.

Animals

C57BL/6JOlaHsd mice were obtained from Harlan UK (Bicester, UK). All animal work was carried out in accordance with the Animals (Scientific Procedures) Act, 1986, under Project License 70/7620.

Cell culture

Explant SCG cultures

SCGs were dissected from 0 to 2 days old C57BL/6 (wild-type) mouse pups. Cleaned explants were placed in the centre of 3.5 cm tissue culture dishes pre-coated with poly-L-lysine (20 mg/mL for 1–2 h; Sigma) and laminin (20 mg/mL for 1–2 h; Sigma). Explants were cultured in Dulbecco's Modified Eagle's Medium (DMEM) with 4,500 mg/L glucose and 110 mg/L sodium pyruvate (Sigma), 2 mM glutamine (Invitrogen), 1% penicillin/streptomycin (Invitrogen), 100 ng/mL 7S NGF (Invitrogen), and 10% fetal bovine serum (Sigma). Four μM aphidicolin (Calbiochem) was used to reduce proliferation and viability of small numbers of non-neuronal cells. Cultures were used after 6 days.

Dissociated SCG cultures

SCG ganglia were dissociated by incubation in 0.025% trypsin (Sigma) in PBS (without $CaCl_2$ and $MgCl_2$) for 30 min followed by 0.2% collagenase type II (Gibco) in PBS for a further 20 min. Ganglia were then gently triturated using a pipette. After a 2 h pre-plating stage to remove non-neuronal cells, 5,000–10,000 dissociated neurons were plated in a 1 cm^2 poly-L-lysine and laminin-coated area in the centre of 3.5 cm ibidi μ-dishes (Thistle Scientific, Glasgow, UK)

for microinjection experiments or in the centre of 3.5 cm tissue culture dishes for analysis by western blotting. Dissociated cultures were maintained the same as explant cultures.

HDAC6 inhibitors treatment

The SCG explants and dissociated cultures were treated for 24 h at 37ºC with compound dosages ranging from 1 μM to 100 μM for toxicity experiments and 1nM to 250 nM for testing the dose-response study of α-tubulin acetylation. For axonal transport rescue experiments, dissociated SCG cultures were treated with either 100 nM T-3796106, 250 nM T-3793168, 1 μM Tubastatin A or an equivalent amount of DMSO.

Plasmid constructs

The S135F and P182L mutations were introduced separately by QuikChange II site-directed mutagenesis (Stratagene) into the complete open reading frame of human HSPB1 isoform cloned into expression vector pCMV-Tag2 (Stratagene). The mito-EGFP construct was kindly provided by Dr Andrea Loreto.

Microinjection

Microinjection was performed using a Zeiss Axiovert 200 microscope with an Eppendorf 5171 transjector and 5246 micromanipulator system and Eppendorf Femtotips. Microinjection mixes of plasmid DNA were prepared in 0.5× PBS(−), passed through a Spin-X filter (Costar, Glasgow, UK) Eppendorf and injected directly into the nuclei of SCG neurons in dissociated cultures. Femtotips were loaded with the microinjection mix and injection was performed using an Eppendorf 5171 transjector and 5246 micromanipulator system on a Zeiss Axiovert 200 microscope. All injections were carried out directly into the nuclei of dissociated SCG neurons. A maximum total DNA concentration of 0.05 μg/μL in the injection mix was used. Forty cells were injected per dish and imaging was performed 12 hours after microinjection.

Western Blotting

Following treatment, ganglia and neurites were collected and washed in PBS with complete, ethylenediaminetetraacetic acid (EDTA)-free protease inhibitor cocktail tablets (Sigma-Aldrich), and lysed directly into 2x Laemmli sample buffer. A total of 10 µL of each sample were separated on a 12% SDS-PAGE and transferred to PVDF membrane (Millipore) using the Bio-Rad Mini-PROTEAN III wet transfer system. Blots were blocked and incubated with primary antibodies overnight (in 1xTBS pH. 8.3, with 0.05% Tween 20 and 5% milk powder or 5% BSA). The antibodies were directed against α-tubulin (1/5,000; ab 15246, Abcam) and acetylated α-tubulin (1/5,000; T7451, Sigma) and detected with mouse-700 (Life Technologies) and rabbit-800 (LI-COR) secondary antibodies. Blots were then scanned and quantified using the Odyssey imaging system (LI-COR Biosciences, Lincoln, North Carolina).

Live imaging of mitochondrial transport and image analysis

Mitochondria were labelled by microinjection of mito-EGFP and their movement along the neurites was recorded with an inverted spinning-disk confocal microscope Olympus IX70 using a 100x 1.49 NA oil immersion objective (Olympus), and controlled with MetaMorph 7.7 software (Molecular Devices). The environment was controlled with a stage top incubator (model INUBG2E-ZILCS; Tokai Hit), set at 37°C and CO_2 set to 5%. Time lapse images of mitochondrial movements were acquired every 1 s for 2 min (120 frames in total). A total of 4-5 movies from different neurons were captured from each culture dish. Individual neurites were straightened using the Straighten plugin in ImageJ software version 1.44 (Rasband, W.S., ImageJ, U. S. National Institutes of Health, Bethesda, MD; http://imagej.nih.gov/ij/, 1997e2012). Transport parameters were determined for individual neurites using the Difference Tracker set of ImageJ plugins 0[60]. The principal output of these plugins is the number of moving particles identified in each frame of the image, normalized to 1000 pixels (Figure 3A).

Human whole blood assay

Study design

In human whole blood assay, whole human blood was collected from healthy volunteers after informed consent at Takeda Pharmaceutical Company Limited. 25 µL of the collected human whole blood was put into each well of a 96-well round-bottom plate. The whole blood was treated with 10 µL of diluted compounds in 10% FBS containing RPMI 1640 medium (Gibco). In the control group, 0.1% DMSO was added as a final concentration. After that, the treated whole blood was incubated at 37°C for 30 minutes at 5% CO_2. Next, 65 µL of RPMI 1640 medium was added onto each well, and the samples were incubated at 37°C for 3.5 hours. T-3796106, T-3793168, and ACY-1215 were dissolved in 100% DMSO (to a stock concentration of 10-300 mM for our in vitro studies).

Measurements

For flow cytometry analyses, the compound-treated whole blood samples were transferred to an assay block (Costar). Diluted Lyse/Fix buffer (BD Biosciences) in dH_2O was added to each sample with pipetting well. The samples were put at RT for 10 minutes and then centrifuged at 400xg for 5 minutes. After centrifugation, the supernatant was removed by aspiration. 250 µL of Perm/Wash buffer I (BD Biosciences) was added to each well and the samples were transferred into a 96-well V-bottom plate, and they were incubated on ice for 20 minutes. These samples were centrifuged at 400xg for 5 minutes at RT, and the supernatant was removed by aspiration. The cells were stained with Zenon conjugated AF647 acetylated α-tubulin (ab179484, Abcam) or matched isotype control (ab172730, Abcam) for 20-30 minutes on ice. Zenon Rabbit IgG Labeling Kit, AF647 (Molecular Probes) was used according to the provided protocol. The cells were centrifuged at 400xg at 5 minutes, and the supernatant was removed, and then washed with 200 µL of Perm/Wash buffer I. After re-centrifugation and removal of the supernatant, the samples were suspended with 200 µL of FACS stain buffer (1% FBS/PBS). The samples were analyzed using lymphocyte gate by BD Fortessa, and the results were analyzed with FlowJo software. Therefore, only lymphocytes were analyzed neither erythrocytes nor thrombocytes were included in the assay.

Statistical analysis

Statistical tests, as described in the figure legends, were performed using Prism software (GraphPad Software Inc, La Jolla, CA, USA). A p value of >0.05 was considered not significant (ns) and *p < 0.05 was significant.

SUPPORTING INFORMATION

Supplementary method and extended western blot results.

AUTHOR INFORMATION

Corresponding Authors

*(M.P.C.) Tel: +44 1223 362151, Fax: +44 1223 331174. E-mail: mc469@cam.ac.uk

*(M.M) Tel/Fax: +44 20 3116 8965. E-mail: mahindra.makhija@takeda.com

Authors Contributions

Research design: R.A., M.T. M., and M.P.C. Experimental work: R.A., A.K, A.L., C.A., X.Y., J.G., T.H., and K.U. Data analyses and interpretation: R.A., A.L., C.A., M. T. M, and M.P.C. Writing the manuscript: R.A., M.P.C. and M.T.M.

Funding

Funding for this work was provided by Takeda Development Centre Europe Ltd. M.P.C. is funded by the John and Lucille van Geest Foundation.

Notes

The authors declare no competing financial interests.

Table of contents was created with BioRender.com.

ACKNOWLEDGMENTS

The authors thank Daniel Curran and Tauhid Ali for their contribution to the discussions; Masashi Toyofuku, Kousuke Hidaka and Fumiaki Kikuchi for the synthesis of T-3796106, T-3793168 and ACY-1215, Andrea Loreto for mito-EGFP construct and Myra Ng for the development of human whole blood assay..

ABBREVIATIONS

HDAC, histone deacetylase; KIF5A, kinesin heavy chain isoform 5A; $A\beta_{1-42}$, amyloid beta peptide 42; HMN, hereditary motor neuropathy; NMNAT2, nicotinamide mononucleotide adenylyltransferase 2; DMSO, dimethyl sulfoxide; FBS, fetal bovine serum.

References

1. Reid, E., Kloos, M., Ashley-Koch, A., Hughes, L., Bevan, S., Svenson, I. K., Graham, F. L., Gaskell, P. C., Dearlove, A., Pericak-Vance, M. A., Rubinsztein, D. C., and Marchuk, D. A. (2002) A kinesin heavy chain (KIF5A) mutation in hereditary spastic paraplegia (SPG10), *Am J Hum Genet 71*, 1189-1194.

2. Crimella, C., Baschirotto, C., Arnoldi, A., Tonelli, A., Tenderini, E., Airoldi, G., Martinuzzi, A., Trabacca, A., Losito, L., Scarlato, M., Benedetti, S., Scarpini, E., Spinicci, G., Bresolin, N., and Bassi, M. T. (2012) Mutations in the motor and stalk domains of KIF5A in spastic paraplegia type 10 and in axonal Charcot-Marie-Tooth type 2, *Clin. Genet. 82*, 157-164.

3. Brenner, D., Yilmaz, R., Muller, K., Grehl, T., Petri, S., Meyer, T., Grosskreutz, J., Weydt, P., Ruf, W., Neuwirth, C., Weber, M., Pinto, S., Claeys, K. G., Schrank, B., Jordan, B., Knehr, A., Gunther, K., Hubers, A., Zeller, D., Kubisch, C., Jablonka, S., Sendtner, M., Klopstock, T., de Carvalho, M., Sperfeld, A., Borck, G., Volk, A. E., Dorst, J., Weis, J., Otto, M., Schuster, J., Del Tredici, K., Braak, H., Danzer, K. M., Freischmidt, A., Meitinger, T., Strom, T. M., Ludolph, A. C., Andersen, P. M., Weishaupt, J. H., and German, A. L. S. n. M. N. D. N. E. T. (2018) Hot-spot KIF5A mutations cause familial ALS, *Brain 141*, 688-697.

4. Nicolas, A., and Kenna, K. P., and Renton, A. E., and Ticozzi, N., and Faghri, F., and Chia, R., and Dominov, J. A., and Kenna, B. J., and Nalls, M. A., and Keagle, P., and Rivera, A. M., and van Rheenen,

W., and Murphy, N. A., and van Vugt, J., and Geiger, J. T., and Van der Spek, R. A., and Pliner, H. A., and Shankaracharya, and Smith, B. N., and Marangi, G., and Topp, S. D., and Abramzon, Y., and Gkazi, A. S., and Eicher, J. D., and Kenna, A., and Consortium, I., and Mora, G., and Calvo, A., and Mazzini, L., and Riva, N., and Mandrioli, J., and Caponnetto, C., and Battistini, S., and Volanti, P., and La Bella, V., and Conforti, F. L., and Borghero, G., and Messina, S., and Simone, I. L., and Trojsi, F., and Salvi, F., and Logullo, F. O., and D'Alfonso, S., and Corrado, L., and Capasso, M., and Ferrucci, L., and Genomic Translation for, A. L. S. C. C., and Moreno, C. A. M., and Kamalakaran, S., and Goldstein, D. B., and Consortium, A. L. S. S., and Gitler, A. D., and Harris, T., and Myers, R. M., and Consortium, N. A., and Phatnani, H., and Musunuri, R. L., and Evani, U. S., and Abhyankar, A., and Zody, M. C., and Answer, A. L. S. F., and Kaye, J., and Finkbeiner, S., and Wyman, S. K., and LeNail, A., and Lima, L., and Fraenkel, E., and Svendsen, C. N., and Thompson, L. M., and Van Eyk, J. E., and Berry, J. D., and Miller, T. M., and Kolb, S. J., and Cudkowicz, M., and Baxi, E., and Clinical Research in, A. L. S., and Related Disorders for Therapeutic Development, C., and Benatar, M., and Taylor, J. P., and Rampersaud, E., and Wu, G., and Wuu, J., and Consortium, S., and Lauria, G., and Verde, F., and Fogh, I., and Tiloca, C., and Comi, G. P., and Soraru, G., and Cereda, C., and French, A. L. S. C., and Corcia, P., and Laaksovirta, H., and Myllykangas, L., and Jansson, L., and Valori, M., and Ealing, J., and Hamdalla, H., and Rollinson, S., and Pickering-Brown, S., and Orrell, R. W., and Sidle, K. C., and Malaspina, A., and Hardy, J., and Singleton, A. B., and Johnson, J. O., and Arepalli, S., and Sapp, P. C., and McKenna-Yasek, D., and Polak, M., and Asress, S., and Al-Sarraj, S., and King, A., and Troakes, C., and Vance, C., and de Belleroche, J., and Baas, F., and Ten Asbroek, A., and Munoz-Blanco, J. L., and Hernandez, D. G., and Ding, J., and Gibbs, J. R., and Scholz, S. W., and Floeter, M. K., and Campbell, R. H., and Landi, F., and Bowser, R., and Pulst, S. M., and Ravits, J. M., and MacGowan, D. J. L., and Kirby, J., and Pioro, E. P., and Pamphlett, R., and Broach, J., and Gerhard, G., and Dunckley, T. L., and Brady, C. B., and Kowall, N. W., and Troncoso, J. C., and Le Ber, I., and Mouzat, K., and Lumbroso, S., and Heiman-Patterson, T. D., and Kamel, F., and Van Den Bosch, L., and Baloh, R. H., and Strom, T. M., and Meitinger, T., and Shatunov, A., and Van Eijk, K. R., and de Carvalho, M., and Kooyman, M., and Middelkoop, B., and Moisse, M., and McLaughlin, R. L., and Van Es, M. A., and Weber, M., and Boylan, K. B., and Van Blitterswijk, M., and Rademakers, R., and Morrison, K. E., and Basak, A. N., and Mora, J. S., and Drory, V. E., and Shaw, P. J., and Turner, M. R., and Talbot, K., and Hardiman, O., and Williams, K. L., and Fifita, J. A., and Nicholson, G. A., and Blair, I. P., and Rouleau, G. A., and Esteban-Perez, J., and Garcia-Redondo, A., and Al-Chalabi, A., and Project Min, E. A. L. S. S. C., and Rogaeva, E., and Zinman, L., and Ostrow, L. W., and Maragakis, N. J., and Rothstein, J. D., and Simmons, Z., and Cooper-Knock, J., and Brice, A., and Goutman, S. A., and Feldman, E. L., and Gibson, S. B., and Taroni, F., and Ratti, A., and Gellera, C., and Van Damme, P., and Robberecht, W., and Fratta, P., and Sabatelli, M., and Lunetta, C., and Ludolph, A. C., and Andersen, P. M., and Weishaupt, J. H., and Camu, W., and Trojanowski, J. Q., and Van Deerlin, V. M., and Brown, R. H., Jr., and van den Berg, L. H., and Veldink, J. H., and Harms, M. B., and Glass, J. D., and Stone, D. J., and Tienari, P., and Silani, V., and Chio, A., and Shaw, C. E., and Traynor, B. J., and Landers, J. E. (2018) Genome-wide Analyses Identify KIF5A as a Novel ALS Gene, *Neuron 97*, 1268-1283 e1266.

5. Duis, J., Dean, S., Applegate, C., Harper, A., Xiao, R., He, W., Dollar, J. D., Sun, L. R., Waberski, M. B., Crawford, T. O., Hamosh, A., and Stafstrom, C. E. (2016) KIF5A mutations cause an infantile onset phenotype including severe myoclonus with evidence of mitochondrial dysfunction, *Ann Neurol 80*, 633-637.

6. Puls, I., Jonnakuty, C., LaMonte, B. H., Holzbaur, E. L., Tokito, M., Mann, E., Floeter, M. K., Bidus, K., Drayna, D., Oh, S. J., Brown, R. H., Jr., Ludlow, C. L., and Fischbeck, K. H. (2003) Mutant dynactin in motor neuron disease, *Nat Genet 33*, 455-456.

7. Puls, I., Oh, S. J., Sumner, C. J., Wallace, K. E., Floeter, M. K., Mann, E. A., Kennedy, W. R., Wendelschafer-Crabb, G., Vortmeyer, A., Powers, R., Finnegan, K., Holzbaur, E. L., Fischbeck, K. H., and Ludlow, C. L. (2005) Distal spinal and bulbar muscular atrophy caused by dynactin mutation, *Ann Neurol 57*, 687-694.

8. Martin, N., Jaubert, J., Gounon, P., Salido, E., Haase, G., Szatanik, M., and Guenet, J. L. (2002) A missense mutation in Tbce causes progressive motor neuronopathy in mice, *Nat Genet 32*, 443-447.

9. Bird, T. D. (1993) Charcot-Marie-Tooth Neuropathy Type 2. In *GeneReviews((R))* (Adam, M. P., Ardinger, H. H., Pagon, R. A., Wallace, S. E., Bean, L. J. H., Stephens, K., and Amemiya, A., Eds.), Seattle (WA).

10. Ismailov, S. M., Fedotov, V. P., Dadali, E. L., Polyakov, A. V., Van Broeckhoven, C., Ivanov, V. I., De Jonghe, P., Timmerman, V., and Evgrafov, O. V. (2001) A new locus for autosomal dominant Charcot-Marie-Tooth disease type 2 (CMT2F) maps to chromosome 7q11-q21, *Eur J Hum Genet 9*, 646-650.

11. d'Ydewalle, C., Krishnan, J., Chiheb, D. M., Van Damme, P., Irobi, J., Kozikowski, A. P., Vanden Berghe, P., Timmerman, V., Robberecht, W., and Van Den Bosch, L. (2011) HDAC6 inhibitors reverse axonal loss in a mouse model of mutant HSPB1-induced Charcot-Marie-Tooth disease, *Nat. Med. 17*, 968-U986.

12. Bakthisaran, R., Tangirala, R., and Rao Ch, M. (2015) Small heat shock proteins: Role in cellular functions and pathology, *Biochim Biophys Acta 1854*, 291-319.

13. Haslbeck, M., and Vierling, E. (2015) A first line of stress defense: small heat shock proteins and their function in protein homeostasis, *J Mol Biol 427*, 1537-1548.

14. Schwartz, N. U. (2019) Charcot-Marie-Tooth 2F (Hsp27 mutations): A review, *Neurobiol Dis 130*, 104505.

15. Evgrafov, O. V., Mersiyanova, I., Irobi, J., Van Den Bosch, L., Dierick, I., Leung, C. L., Schagina, O., Verpoorten, N., Van Impe, K., Fedotov, V., Dadali, E., Auer-Grumbach, M., Windpassinger, C., Wagner, K., Mitrovic, Z., Hilton-Jones, D., Talbot, K., Martin, J. J., Vasserman, N., Tverskaya, S., Polyakov, A., Liem, R. K., Gettemans, J., Robberecht, W., De Jonghe, P., and Timmerman, V. (2004) Mutant small heat-shock protein 27 causes axonal Charcot-Marie-Tooth disease and distal hereditary motor neuropathy, *Nat Genet 36*, 602-606.

16. Juneja, M., Burns, J., Saporta, M. A., and Timmerman, V. (2019) Challenges in modelling the Charcot-Marie-Tooth neuropathies for therapy development, *J Neurol Neurosurg Psychiatry 90*, 58-67.

17. Almeida-Souza, L., Goethals, S., de Winter, V., Dierick, I., Gallardo, R., Van Durme, J., Irobi, J., Gettemans, J., Rousseau, F., Schymkowitz, J., Timmerman, V., and Janssens, S. (2010) Increased

monomerization of mutant HSPB1 leads to protein hyperactivity in Charcot-Marie-Tooth neuropathy, *J Biol Chem 285*, 12778-12786.

18. Lee, J., Jung, S. C., Joo, J., Choi, Y. R., Moon, H. W., Kwak, G., Yeo, H. K., Lee, J. S., Ahn, H. J., Jung, N., Hwang, S., Rheey, J., Woo, S. Y., Kim, J. Y., Hong, Y. B., and Choi, B. O. (2015) Overexpression of mutant HSP27 causes axonal neuropathy in mice, *J Biomed Sci 22*, 43.

19. Bouhy, D., Geuens, T., De Winter, V., Almeida-Souza, L., Katona, I., Weis, J., Hochepied, T., Goossens, S., Haigh, J. J., Janssens, S., and Timmerman, V. (2016) Characterization of New Transgenic Mouse Models for Two Charcot-Marie-Tooth-Causing HspB1 Mutations using the Rosa26 Locus, *J Neuromuscul Dis 3*, 183-200.

20. Srivastava, A. K., Renusch, S. R., Naiman, N. E., Gu, S., Sneh, A., Arnold, W. D., Sahenk, Z., and Kolb, S. J. (2012) Mutant HSPB1 overexpression in neurons is sufficient to cause age-related motor neuronopathy in mice, *Neurobiol Dis 47*, 163-173.

21. Hoke, A., and Ray, M. (2014) Rodent models of chemotherapy-induced peripheral neuropathy, *ILAR journal 54*, 273-281.

22. LaPointe, N. E., Morfini, G., Brady, S. T., Feinstein, S. C., Wilson, L., and Jordan, M. A. (2013) Effects of eribulin, vincristine, paclitaxel and ixabepilone on fast axonal transport and kinesin-1 driven microtubule gliding: Implications for chemotherapy-induced peripheral neuropathy, *Neurotoxicology 37*, 231-239.

23. Trinczek, B., Ebneth, A., Mandelkow, E. M., and Mandelkow, E. (1999) Tau regulates the attachment/detachment but not the speed of motors in microtubule-dependent transport of single vesicles and organelles, *J Cell Sci 112 (Pt 14)*, 2355-2367.

24. Dixit, R., Ross, J. L., Goldman, Y. E., and Holzbaur, E. L. (2008) Differential regulation of dynein and kinesin motor proteins by tau, *Science 319*, 1086-1089.

25. Vossel, K. A., Zhang, K., Brodbeck, J., Daub, A. C., Sharma, P., Finkbeiner, S., Cui, B., and Mucke, L. (2010) Tau reduction prevents Abeta-induced defects in axonal transport, *Science 330*, 198.

26. Adalbert, R., Milde, S., Durrant, C., Ando, K., Stygelbout, V., Yilmaz, Z., Gould, S., Brion, J. P., and Coleman, M. P. (2018) Interaction between a MAPT variant causing frontotemporal dementia and mutant APP affects axonal transport, *Neurobiol Aging 68*, 68-75.

27. Stokin, G. B., Lillo, C., Falzone, T. L., Brusch, R. G., Rockenstein, E., Mount, S. L., Raman, R., Davies, P., Masliah, E., Williams, D. S., and Goldstein, L. S. (2005) Axonopathy and transport deficits early in the pathogenesis of Alzheimer's disease, *Science 307*, 1282-1288.

28. De Vos, K. J., and Hafezparast, M. (2017) Neurobiology of axonal transport defects in motor neuron diseases: Opportunities for translational research?, *Neurobiol Dis*.

29. Smith, A. L., Teener, J. W., Callaghan, B. C., Harrington, J., and Uhlmann, W. R. (2014) Amyotrophic lateral sclerosis in a patient with a family history of huntington disease: genetic counseling challenges, *Journal of genetic counseling 23*, 725-733.

30. Ittner, L. M., Fath, T., Ke, Y. D., Bi, M., van Eersel, J., Li, K. M., Gunning, P., and Gotz, J. (2008) Parkinsonism and impaired axonal transport in a mouse model of frontotemporal dementia, *Proc Natl Acad Sci U S A 105*, 15997-16002.

31. Alami, N. H., Smith, R. B., Carrasco, M. A., Williams, L. A., Winborn, C. S., Han, S. S. W., Kiskinis, E., Winborn, B., Freibaum, B. D., Kanagaraj, A., Clare, A. J., Badders, N. M., Bilican, B., Chaum, E., Chandran, S., Shaw, C. E., Eggan, K. C., Maniatis, T., and Taylor, J. P. (2014) Axonal transport of TDP-43 mRNA granules is impaired by ALS-causing mutations, *Neuron 81*, 536-543.

32. Adalbert, R., and Coleman, M. P. (2013) Review: Axon pathology in age-related neurodegenerative disorders, *Neuropathol Appl Neurobiol 39*, 90-108.

33. Milde, S., Adalbert, R., Elaman, M. H., and Coleman, M. P. (2015) Axonal transport declines with age in two distinct phases separated by a period of relative stability, *Neurobiol Aging 36*, 971-981.

34. Stepanova, T., Slemmer, J., Hoogenraad, C. C., Lansbergen, G., Dortland, B., De Zeeuw, C. I., Grosveld, F., van Cappellen, G., Akhmanova, A., and Galjart, N. (2003) Visualization of microtubule growth in cultured neurons via the use of EB3-GFP (end-binding protein 3-green fluorescent protein), *J Neurosci 23*, 2655-2664.

35. Baas, P. W., and Qiang, L. (2005) Neuronal microtubules: when the MAP is the roadblock, *Trends Cell Biol 15*, 183-187.

36. Yu, W., and Baas, P. W. (1994) Changes in microtubule number and length during axon differentiation, *J Neurosci 14*, 2818-2829.

37. Portran, D., Schaedel, L., Xu, Z., Thery, M., and Nachury, M. V. (2017) Tubulin acetylation protects long-lived microtubules against mechanical ageing, *Nat Cell Biol 19*, 391-398.

38. Sudo, H., and Baas, P. W. (2010) Acetylation of microtubules influences their sensitivity to severing by katanin in neurons and fibroblasts, *J Neurosci 30*, 7215-7226.

39. Reed, N. A., Cai, D., Blasius, T. L., Jih, G. T., Meyhofer, E., Gaertig, J., and Verhey, K. J. (2006) Microtubule acetylation promotes kinesin-1 binding and transport, *Curr Biol 16*, 2166-2172.

40. Chen, S., Owens, G. C., Makarenkova, H., and Edelman, D. B. (2010) HDAC6 regulates mitochondrial transport in hippocampal neurons, *PloS one 5*, e10848.

41. North, B. J., Marshall, B. L., Borra, M. T., Denu, J. M., and Verdin, E. (2003) The human Sir2 ortholog, SIRT2, is an NAD+-dependent tubulin deacetylase, *Mol Cell 11*, 437-444.

42. Benoy, V., Van Helleputte, L., Prior, R., d'Ydewalle, C., Haeck, W., Geens, N., Scheveneels, W., Schevenels, B., Cader, M. Z., Talbot, K., Kozikowski, A. P., Vanden Berghe, P., Van Damme, P., Robberecht, W., and Van Den Bosch, L. (2018) HDAC6 is a therapeutic target in mutant GARS-induced Charcot-Marie-Tooth disease, *Brain 141*, 673-687.

43. Guo, W. T., Naujock, M., Fumagalli, L., Vandoorne, T., Baatsen, P., Boon, R., Ordovas, L., Patel, A., Welters, M., Vanwelden, T., Geens, N., Tricot, T., Benoy, V., Steyaert, J., Lefebvre-Omar, C., Boesmans, W., Jarpe, M., Sterneckert, J., Wegner, F., Petri, S., Bohl, D., Vanden Berghe, P., Robberecht, W., Van Damme, P., Verfaillie, C., and Van den Bosch, L. (2017) HDAC6 inhibition reverses axonal transport defects in motor neurons derived from FUS-ALS patients, *Nature communications 8*.

44. Van Helleputte, L., Kater, M., Cook, D. P., Eykens, C., Rossaert, E., Haeck, W., Jaspers, T., Geens, N., Berghe, P. V., Gysemans, C., Mathieu, C., Robberecht, W., Van Damme, P., Cavaletti, G., Jarpe, M., and Van Den Bosch, L. (2018) Inhibition of histone deacetylase 6 (HDAC6) protects against vincristine-induced peripheral neuropathies and inhibits tumor growth, *Neurobiol. Dis. 111*, 59-69.

45. Zhang, L., Liu, C., Wu, J., Tao, J. J., Sui, X. L., Yao, Z. G., Xu, Y. F., Huang, L., Zhu, H., Sheng, S. L., and Qin, C. (2014) Tubastatin A/ACY-1215 Improves Cognition in Alzheimer's Disease Transgenic Mice, *Journal of Alzheimers Disease 41*, 1193-1205.

46. Wang, Z., Leng, Y., Wang, J., Liao, H. M., Bergman, J., Leeds, P., Kozikowski, A., and Chuang, D. M. (2016) Tubastatin A, an HDAC6 inhibitor, alleviates stroke-induced brain infarction and functional deficits: potential roles of alpha-tubulin acetylation and FGF-21 up-regulation, *Scientific reports 6*, 19626.

47. Butler, K. V., Kalin, J., Brochier, C., Vistoli, G., Langley, B., and Kozikowski, A. P. (2010) Rational design and simple chemistry yield a superior, neuroprotective HDAC6 inhibitor, tubastatin A, *J. Am. Chem. Soc. 132*, 10842-10846.

48. Benoy, V., Vanden Berghe, P., Jarpe, M., Van Damme, P., Robberecht, W., and Van Den Bosch, L. (2017) Development of Improved HDAC6 Inhibitors as Pharmacological Therapy for Axonal Charcot-Marie-Tooth Disease, *Neurotherapeutics : the journal of the American Society for Experimental NeuroTherapeutics 14*, 417-428.

49. He, J. C., Yao, W., Wang, J. M., Schemmer, P., Yang, Y., Liu, Y., Qian, Y. W., Qi, W. P., Zhang, J., Shen, Q., and Yang, T. (2016) TACC3 overexpression in cholangiocarcinoma correlates with poor

prognosis and is a potential anti-cancer molecular drug target for HDAC inhibitors, *Oncotarget 7*, 75441-75456.

50. Flipo, M., Charton, J., Hocine, A., Dassonneville, S., Deprez, B., and Deprez-Poulain, R. (2009) Hydroxamates: relationships between structure and plasma stability, *J. Med. Chem. 52*, 6790-6802.

51. Gilley, J., and Coleman, M. P. (2010) Endogenous Nmnat2 is an essential survival factor for maintenance of healthy axons, *PLoS Biol 8*, e1000300.

52. Milde, S., Gilley, J., and Coleman, M. P. (2013) Axonal trafficking of NMNAT2 and its roles in axon growth and survival in vivo, *Bioarchitecture 3*, 133-140.

53. Santo, L., Hideshima, T., Kung, A. L., Tseng, J. C., Tamang, D., Yang, M., Jarpe, M., van Duzer, J. H., Mazitschek, R., Ogier, W. C., Cirstea, D., Rodig, S., Eda, H., Scullen, T., Canavese, M., Bradner, J., Anderson, K. C., Jones, S. S., and Raje, N. (2012) Preclinical activity, pharmacodynamic, and pharmacokinetic properties of a selective HDAC6 inhibitor, ACY-1215, in combination with bortezomib in multiple myeloma, *Blood 119*, 2579-2589.

54. Maday, S., Wallace, K. E., and Holzbaur, E. L. (2012) Autophagosomes initiate distally and mature during transport toward the cell soma in primary neurons, *J Cell Biol 196*, 407-417.

55. Misgeld, T., Kerschensteiner, M., Bareyre, F. M., Burgess, R. W., and Lichtman, J. W. (2007) Imaging axonal transport of mitochondria in vivo, *Nat Methods 4*, 559-561.

56. Gibbs, K. L., Kalmar, B., Sleigh, J. N., Greensmith, L., and Schiavo, G. (2016) In vivo imaging of axonal transport in murine motor and sensory neurons, *J Neurosci Methods 257*, 26-33.

57. Zhang, B., Maiti, A., Shively, S., Lakhani, F., McDonald-Jones, G., Bruce, J., Lee, E. B., Xie, S. X., Joyce, S., Li, C., Toleikis, P. M., Lee, V. M., and Trojanowski, J. Q. (2005) Microtubule-binding drugs offset tau sequestration by stabilizing microtubules and reversing fast axonal transport deficits in a tauopathy model, *Proc Natl Acad Sci U S A 102*, 227-231.

58. Lin, M. Y., Cheng, X. T., Tammineni, P., Xie, Y., Zhou, B., Cai, Q., and Sheng, Z. H. (2017) Releasing Syntaphilin Removes Stressed Mitochondria from Axons Independent of Mitophagy under Pathophysiological Conditions, *Neuron 94*, 595-610 e596.

59. Kaieda A, T. M., Daini M, Nara H, Yoshikawa M, Ishii N, Hidaka K,. (2017) Oxadiazole derivatives useful as HDAC inhibitors. Patent WO2017014321.

60. Andrews, S., Gilley, J., and Coleman, M. P. (2010) Difference Tracker: ImageJ plugins for fully automated analysis of multiple axonal transport parameters, *J Neurosci Methods 193*, 281-287.

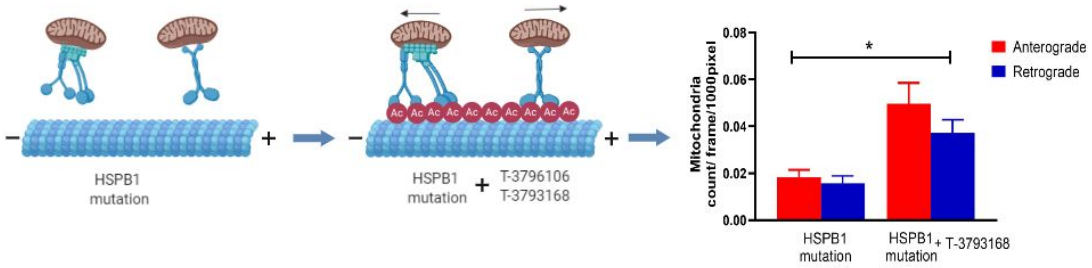

For table of contents only

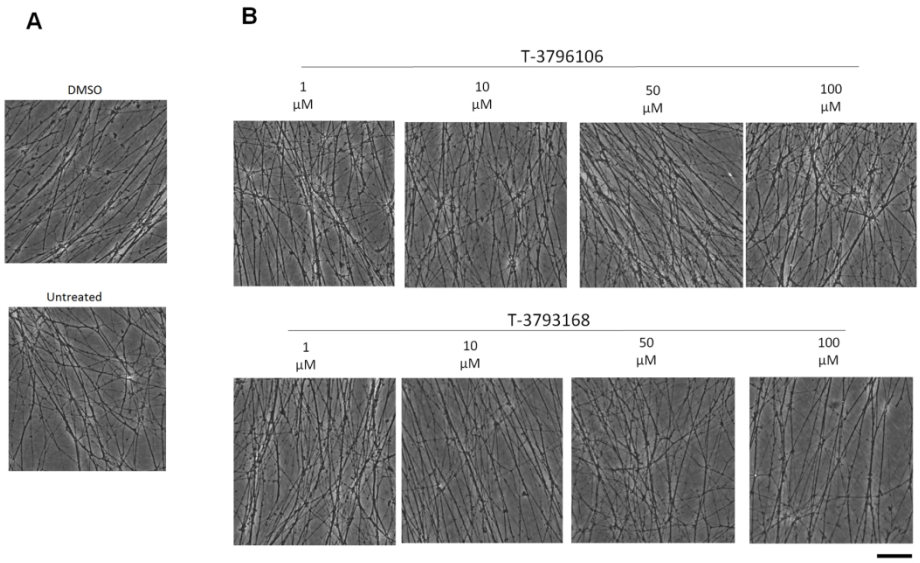

Figure 1

Figure 1. Morphologically normal neurites of SCG explants treated with high concentrations of T-3796106 and T-3793168. (A) Vehicle treated and untreated cultures have healthy looking neurites with no signs of fragmentation or blebbing. (B) Cultures treated with indicated compound concentrations look morphologically similar with control cultures, which suggest no cytotoxic effect. Scale bar 50 μm.

168x117mm (300 x 300 DPI)

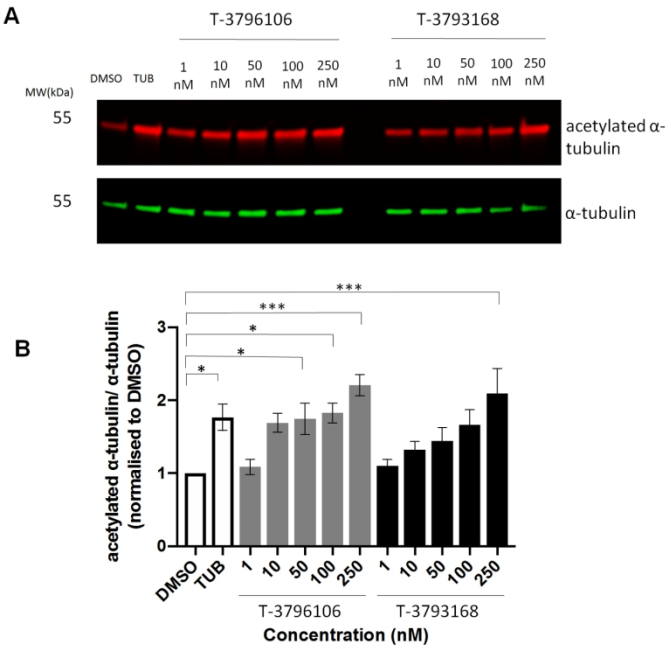

Figure 2

Figure 2. Pharmacological properties of T-3796106 and T-3793168 in SCG neurons. Western blot showing dose response of T-3796106 and T-3793168 (A) on acetylation of α-tubulin. 1 μM Tubastatin A (Tub) was used as positive control. Quantification of the ratio of acetylated α-tubulin to total tubulin levels on Western blot for T-3796106 and T-3793168 (B). Statistically significant difference between groups is indicated (*$p < 0.05$, 1-way analysis of variance). Data are presented as means ± s.e.m. n=4-5.

168x117mm (300 x 300 DPI)

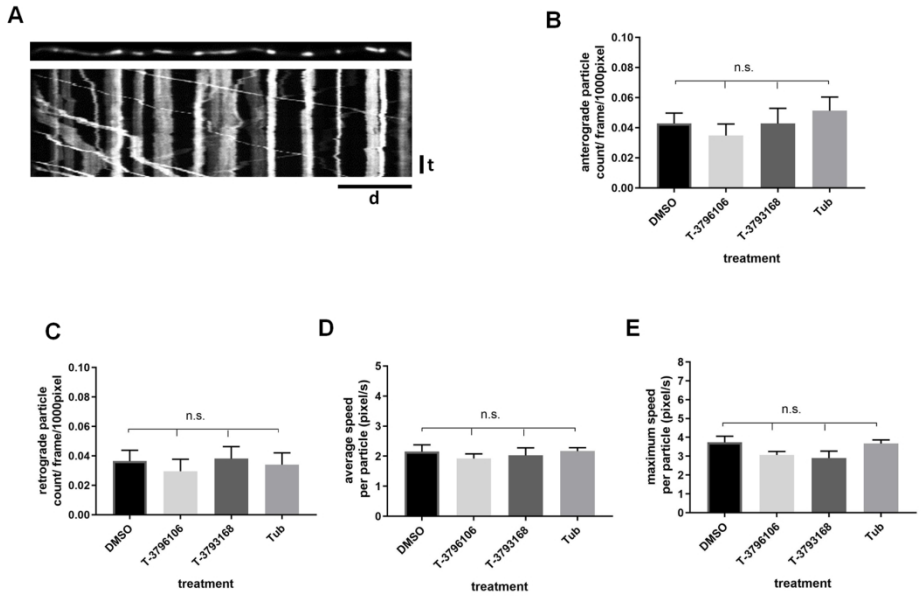

Figure 3

Figure 3. Mitochondrial transport remains unaltered in wild type SCGs after treatment. Representative kymograph obtained from a SCG neuron grown in dissociated cultures (A). The top image shows a straightened neurite. Vertical lines indicate stationary mitochondria while lines deflecting to the right or left represent anterograde or retrograde moving mitochondria. Time (t) scale bar: 120 s; distance (d) scale bar: 10 µm. Quantification of anterograde (B) and retrograde (C) mitochondria transport, average (D) and maximum speed (E) of mitochondria movement in neurons treated with the indicated compounds and concentrations. Data are presented as means ± s.e.m. n=12-14.

168x117mm (300 x 300 DPI)

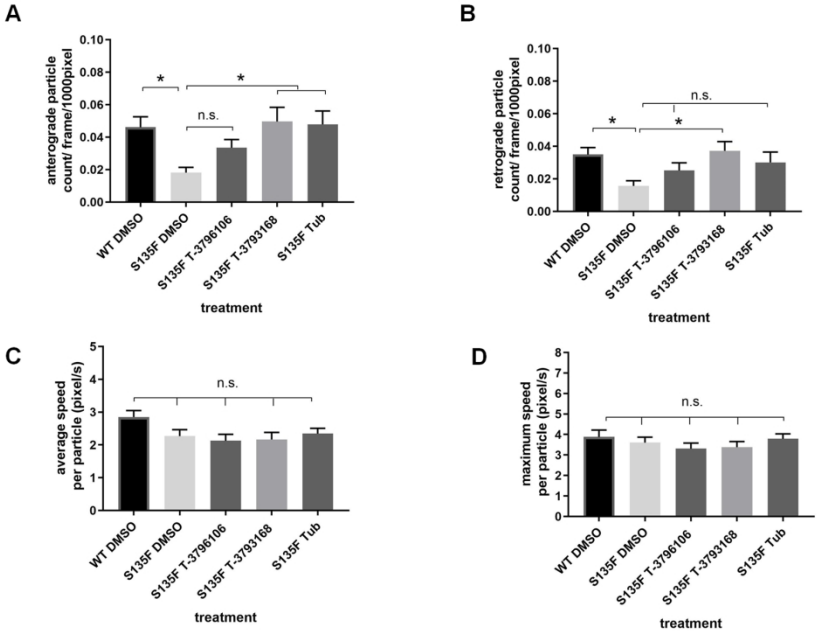

Figure 4

Figure 4. T-3793168 reverses axonal transport deficit in SCGs with HSPB1S135F mutation. Quantification of anterograde (A) and retrograde (B) mitochondria transport, average (C) and maximum speed (D) of movement with genotypes and treatments indicated. Statistically significant differences between groups is indicated (*$p < 0.05$, 1-way analysis of variance). Data are presented as means ± s.e.m. n=12-17.

168x117mm (300 x 300 DPI)

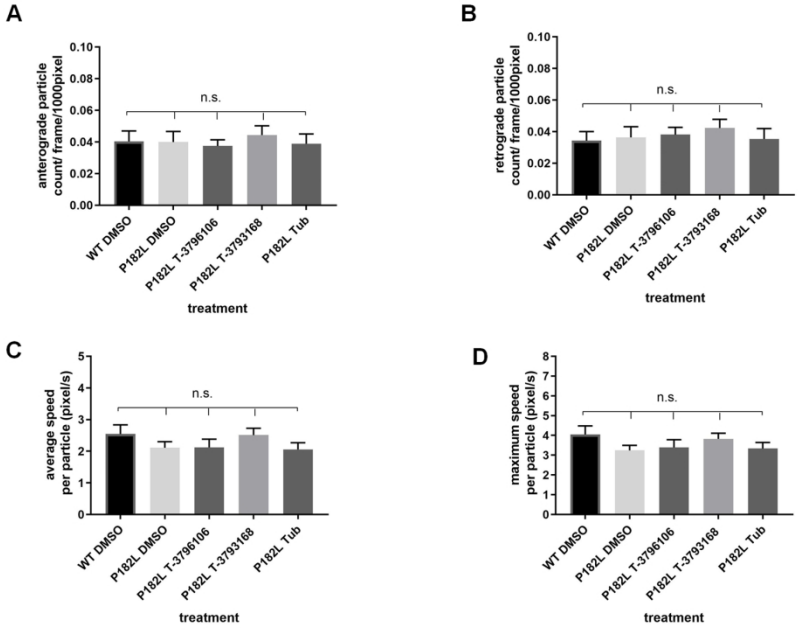

Figure 5

Figure 5. No changes in axonal transport of SCGs with HSPB1P182L mutation. Quantification of anterograde (A), retrograde (B), average (C) and maximum speed (D) of mitochondria transport with genotypes and treatments indicated. Data are presented as means ± s.e.m. n=12-14.

168x117mm (300 x 300 DPI)

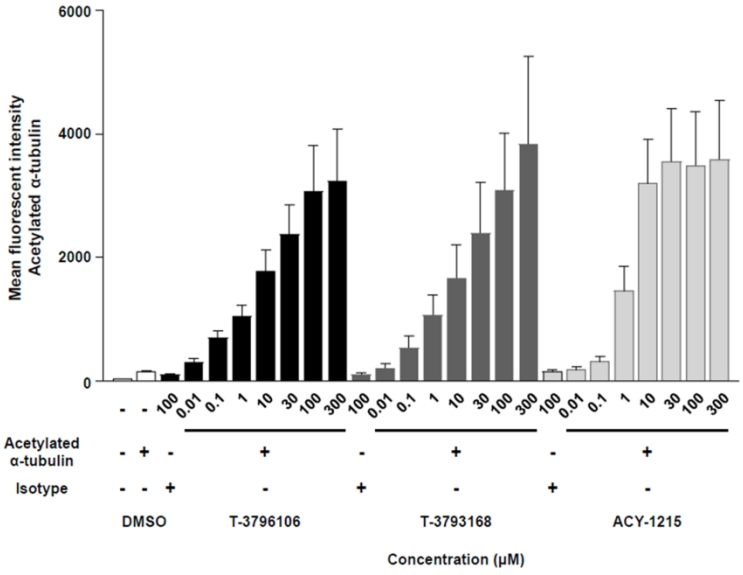

Figure 6

Figure 6. Increased acetylation levels of α-tubulin in human whole blood. Quantification of acetylated α-tubulin in whole blood treated with the indicated compounds and concentrations. Data are presented as means ± s.e.m. n=3.

168x117mm (300 x 300 DPI)